RSC Advances

PAPER

Cite this: *RSC Adv.*, 2016, **6**, 105862

# Acetyl salicylic acid–ZnAl layered double hydroxide functional nanohybrid for skin care application

Damodar Mosangi,[abc] Lumbidzani Moyo,[a] Sreejarani Kesavan Pillai[a] and Suprakas Sinha Ray*[ab]

Received 4th September 2016
Accepted 27th October 2016

DOI: 10.1039/c6ra22172f

www.rsc.org/advances

In this study, a pharmaceutically active ingredient, acetyl salicylic acid (ASA), was intercalated into ZnAl layered double hydroxide (LDH). The LDH–ASA nanohybrid material was characterized by XRD, FTIR, SEM, ICP-MS, TEM and TGA. Successful incorporation of ASA into LDH interlayers through electrostatic interactions was confirmed by FTIR results. ASA in the intercalated form showed higher thermal stability in comparison to pure ASA. *In vitro* release studies revealed that the nanohybrid in release media (artificial sweat/phosphate-buffered saline) could effectively facilitate the ASA diffusion by significantly increasing the release time. The nanohybrid was also used to develop a topical skin care formulation, and skin permeation kinetic studies were conducted by a Franz diffusion cell using reconstructed skin samples. The results from the Franz diffusion cell experiments showed that the formulation with the LDH–ASA nanohybrid drastically increased the penetration rate for ASA compared to the formulation with pure ASA. From these studies, we can conclude that the *in situ* intercalation of an LDH–ASA nanohybrid system is a promising alternative active ingredient for topical cosmetic emulsions.

## 1 Introduction

Recently, the incorporation of inorganic/organic anions into layered inorganic matrices has presented an interesting opportunity to develop new nanohybrid materials, which have great practical importance in pharmaceuticals, catalysis and magnetic precursor fields.[1] Among various layered inorganic matrices used in a variety of multidisciplinary fields, layered double hydroxides (LDHs), which are referred to as hydrotalcite-like compounds or anionic clays, hold great interest as effective nanocarriers for the delivery of pharmaceutical drugs, biomedical actives, genes and so on.[2–5] LDHs with empirical formula $[M_{(1-x)}^{2+}M_x^{3+}(OH)_2]^{x+}(A_{(x/n)}^{n-})\cdot mH_2O$, consist of brucite-like layers of magnesium hydroxide, where some divalent ($M^{2+}$) cations are isomorphically substituted with trivalent ($M^{3+}$) cations to give the layers a net positive charge. These charges are counter balanced by interlayer anions ($A^{n-}$) such as $CO_3^{2-}$, $Cl^-$, $NO_3^-$.[4] LDHs possess high anion exchange capacity and hence a large variety of inorganic/organic anions can be interchanged and sheltered between the brucite-like layers resulting in nanohybrids that can slowly release active ingredients.[5,6] Previous studies by Ambrogi *et al.*[7–9] showed that the intercalation of pharmaceutical anti-inflammatory drugs, such as indomethacin, ketoprofen, diclofenac and flurbiprofen with LDHs, could be used for developing sustained drug release systems. Choy *et al.*[10,11] reported successful intercalation of anticancer folic acid derivatives such as folinic acid, methotrexate as well as vitamins with LDHs and obtained controlled release properties and protection of molecules from light and heat. Wei and co-workers[12] demonstrated enhanced chemical and stereo-chemical stability of chiral drug L-dopa after intercalation into LDHs.

Unfortunately, there is only little information on whether this protective and controlled release functions of LDHs can be made use for cosmetic or topical applications, where chemically and optically unstable active ingredients are often used.[13–18] LDHs have many attractive features suitable for topical applications namely: skin compatibility, high surface area and adsorption ability to remove skin exudates, high anion exchange ability to protect the active ingredients and release them in a controlled fashion.[13,14] This observation is further confirmed by Yang *et al.*,[15] according to whom intercalating with LDH and further encapsulating with silica nano-sol improved the storage stability and controlled release of vitamin C. The US patent by Choy and group,[16] describes the preparation method for LDH based hybrid materials with active component selected from the group consisting of lactic acid, citric acid, kojic acid, indol-3-acetic acid, *etc.*, for possible application in cosmetics. Perioli and co-workers[17,18] reported the use of LDHs to improve the photo-stability and prevent photo-degradation of sunscreen agent *p*-amino benzoic acid

[a]*DST/CSIR National Centre for Nanostructured Materials, Council for Scientific and Industrial Research, Pretoria 0001, South Africa. E-mail: rsuprakas@csir.co.za; suprakas73@csir.co.za*

[b]*Department of Applied Chemistry, University of Johannesburg, Droonfontein 2028, Johannesburg, South Africa*

[c]*AMKA Products Pty Limited, Innovation Building, 14 Ellman Street, Sunderland Ridge, Centurion 0157, Pretoria, South Africa*

and 2-phenyl-1H-benzimidazole-5-sulfonic acid. In a successive work, Ambrogi *et al.*[19] intercalated a skin whitening ingredient-kojic acid into the interlayers of ZnAl-LDH and the intercalation compound was further formulated to water–oil emulsion that showed good *in vitro* release and photo-stability of the active ingredient. In a recent work, Perioli's group[20] developed gel containing LDH–retinoic acid hybrid for topical treatment of acne vulgaris and observed enhanced photo stability and slow release of retinoic acid.

Acetyl salicylic acid (ASA) is a salicylate derivative which possesses anti-inflammatory effect.[21,22] ASA is generally used for pain relief in topical after shave skincare products. However, it becomes less effective and develops undesirable smell as it undergoes hydrolysis into salicylic and acetic acids in presence of moisture or water.[23] Therefore its stability is often the initial apprehension in formulation development. ASA is an aromatic organic molecule with an easily polarizable carboxylic group (refer Fig. 1), thus allowing the intercalation of anions between the brucite-like layers of LDHs.

Although a few studies are available on ASA intercalated LDH nanohybrids,[22,24,25] all of them report pharmaceutical applications for improving therapeutic efficiency of orally administered ASA. For instance, to address the severe irritation of gastrointestinal tract and related adverse effects associated with oral administration of ASA, Gou *et al.*,[22] assembled LDH loaded with ASA and provided protective layer with dextran (polysaccharide)[24] to eliminate acid corrosion of LDH layers in intestinal acidic conditions. The pharma-kinetic study results of the delivery system in rabbit indicated 5-fold increase in half-life of ASA as well as 2-fold increase in oral bioavailability while reducing the adverse effects. Meng *et al.*[25] intercalated ASA into Zn–Al LDH by co-precipitation and reconstruction methods and compared their release behavior experimentally and theoretically. According to them, the nanohybrid synthesized by co-precipitation method showed strong interaction between the LDH layers and hence slow release properties. The facts that ASA is also used widely in topically administered formulations and no reports are available on transdermal LDH–ASA based delivery system. This observation prompted us to investigate the properties of ASA-intercalated LDH nanohybrids' controlled release and stability with the eventual goal of developing a topical cosmetic formulation.

In this study, LDH–ASA nanohybrids were prepared using the co-precipitation technique. The co-precipitation improves the intercalation of ASA because metal hydroxide sheets form stable conformations due to both inter- and intra-molecular interactions. Moreover, the procedure is easy to scale up from the commercialization perspective. *In vitro* release of ASA from nanohybrids was followed by UV-Vis spectroscopy. Finally, the nanohybrid was used for the development of a topical skin care formulation, and skin penetration studies were conducted by a Franz diffusion cell using artificial skin samples. Preliminary *in vivo* studies were also conducted to screen the efficacy of the skin care formulation.

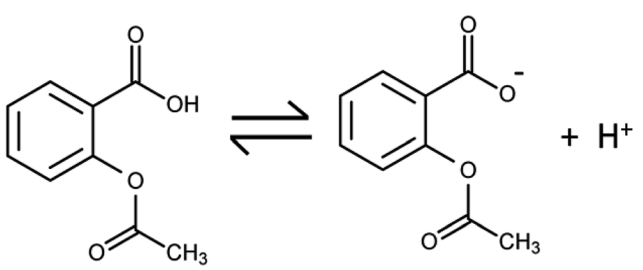


Fig. 1 Chemical structure of ASA and corresponding anion.

## 2 Experimental sections

### Materials

Aluminum chloride hexahydrate ($AlCl_3 \cdot 6H_2O$) (99%), zinc chloride ($ZnCl_2$) (98%) and sodium hydroxide (98%) were obtained from Sigma-Aldrich (South Africa); ASA (100%) from Rhodia (France); propylene glycol from Dow chemicals (USA); EDTA, xantghan gum, triethanol amine (99%) allantoin, vitamin E, glycerol monostearate from IMCD (South Africa), carbomer from Lubrazol (Europe); potassium lactate from Purac (Europe); cetaryalcohol from Ecogreen (Malaysia); isopropyl palmitate from Intermed (Malaysia); sterylcaprolate and heptonate from Symrise (Germany); octyldodecanol and ceteareth-20 from BASF (Germany); vitamin $B_3$ from DSM (Switzerland); dimethicone from Dowcorning (USA); iodopropynyl butylcarbamate and methylisothizolinone from Thor Personal Care (UK), and polyacrylamide, C13-14 isoparaffin and Laureth-7 from Seppic (Europe).

### Synthesis of ZnAl LDH and LDH–ASA nanohybrid

The LDH–ASA nanohybrid was prepared according to our previous report.[26] A brief procedure is as follows: 100 mL solution containing 2 M $ZnCl_2$ and 1 M $AlCl_3 \cdot 6H_2O$ was added to a 80 mL of 1 M solution of ASA in ethanol. 1 M NaOH was added drop-wise under constant stirring, while adjusting the pH to 9–10. The stirring was continued until solutions were completely mixed, after which the precipitate was filtered and washed with a large volume of de-ionized water until all the $Cl^-$ ions were removed. The obtained solid was allowed air-dry overnight before drying in an oven at 70 °C for 24 h. The dried sample was then ground into a powder and sieved to 80 μm particle size for further analysis. ZnAl LDH was prepared as a reference material using a similar procedure in the absence of ASA.

### Development of a topical formulation containing a LDH–ASA nanohybrid

Topical skin formulations were prepared using the ingredients shown in Table 1. Both the oil phase containing a LDH–ASA nanohybrid (concentration of nanohybrid equivalent to 2% ASA content was used) and water phases were heated to 70 °C. After both phases reached the desired temperature, the oil phase was combined into the water phase and mixed for 5 min with a high shear silverson homogenizer. The neutralizer was then added, and the whole mixture was then mixed for another 5 min with the same homogenizer at 3000 rpm. The mixture was cooled to 40 °C and a preservative was added to obtain the LDH–ASA

based emulsion. The pH of the final formulation was adjusted to 5.6. The same procedure was followed for the formulation with pure ASA, where 2% concentration of ASA corresponding to commercial after shave formulation was used. The stability of the formulations was checked at ambient, 37 °C and 50 °C for 4 weeks and no phase separation was found.

### Nanohybrid characterization

X-ray diffraction (XRD) studies were conducted using an X'Pert PRO X-ray diffractometer (PANalytical, Netherlands) operating with Cu K-$\alpha$ radiation (wavelength of 0.15406 nm) at 45 kV and 40 mA. The exposure time and scan speed for the XRD measurements were 19.7 min and 0.036987° per s, respectively. ASA intercalation into the LDHs was followed using Fourier transform infrared (FTIR) spectroscopy (Perkin-Elmer Spectrum 100 spectrometer, USA) with the MIRacle ATR attachment and a Zn/Se plate. A small amount of sample was pressed onto the Zn/Se plate and spectra over the range of 550 to 4000 $cm^{-1}$ were collected. Morphological characteristics of neat LDHs and ASA-intercalated LDHs were obtained using scanning electron microscopy (SEM, JEOL, JSM 7500F, Japan) at 3 kV acceleration voltage. ICP-MS was used to determine the elemental composition of the LDH–ASA. 500 mg of LDH-ASA were leached in an aqua regia solution. The aliquot was left to cool and further diluted with deionised water. These were then analyzed on a Thermo Scientific – iCAP Q Inductively Coupled Plasma Mass Spectrometer (ICP-MS) to quantify the amount of Zn and Al present. Calibration was carried out using internal standard method using scandium (ICP grade). Each sample was measured 3 times and the average ICP-MS value was recorded. The fractional replacement of Zn by Al ions in the hydroxide sheets is quantified by $x$ and is calculated from the equation below:

$$x = \frac{\mathrm{M}\ (\%\%\mathrm{III})}{\mathrm{M}(\%\%\mathrm{II}) + \mathrm{M}(\%\%\mathrm{III})} \quad (1)$$

where M(II) and M(III) are the divalent and trivalent cations, respectively. High-resolution transmission electron microscopy (JEOL JEM 2100 HRTEM, Japan) operated at 200 kV acceleration voltage was used to study the size and shape of the particles. For TEM analysis, the powder samples were sonicated in ethanol for 1 min and dropped on a carbon coated Cu-grid and dried. Thermogravimetric analysis of neat LDHs, ASA, and LDH–ASA nanohybrid were performed using thermogravimetric analyzer (TGA, TA instruments, model Q500, USA). The temperature was ramped at 10°C $min^{-1}$ in air, from 25 °C to 900 °C. The ASA loading capacity of LDH was determined from the residue weight percentage analysis.

### *In vitro* release studies

To measure the amount of ASA released from the LDH–ASA nanohybrids, *in vitro* release tests were performed in two different media. 0.02 g of the LDH–ASA nanohybrid was added separately into a 200 mL artificial sweat (pH 5.4) and phosphate-buffered saline (PBS, dulbeccos buffer without calcium magnesium and sodium bicarbonate obtained from Life Technologies™, France, pH 7.2) solution in a closed beaker at a 37 °C. The artificial sweat was prepared by reported procedure.[27] At regular time intervals after the addition of the nanohybrid, 5 mL of solution (the volume of artificial sweat and PBS was maintained by adding fresh media) was withdrawn and filtered using a PVDF micro syringe filter. The concentration of ASA was measured by UV-Vis spectroscopy (Perkin Elmer Lamda 750, USA) at $\lambda_{max} = 296$ nm. The release profiles were plotted with time *vs.* absorbance. The data were collected in triplicate.

Table 1 Constituents of the formulations used in the current study

| Entry | Ingredients | % |
|---|---|---|
| 1 | Deionized water | QS |
| 2 | Propylene glycol | 10.4 |
| 3 | Nanohybrid | 7.4 |
| 4 | Octyldodecanol | 3.8 |
| 5 | Isopropylpalmitate | 3.4 |
| 6 | Sterylcaprylate | 1.6 |
| 7 | Sterylheptonate | 1.6 |
| 8 | Ceteareth-20 | 1.3 |
| 9 | Cetearyl alcohol | 1.0 |
| 10 | Vitamin B3 | 0.8 |
| 11 | Dimethicone | 0.8 |
| 12 | Glycerol monostearate | 0.7 |
| 13 | Allantoin | 0.4 |
| 14 | Potassium lactate | 0.3 |
| 15 | Triethanal amine | 0.3 |
| 16 | Carbomer | 0.25 |
| 17 | Xanthan gum | 0.2 |
| 18 | $EDTANa_2$ | 0.1 |
| 19 | Vitamin E | 0.1 |
| 20 | Iodopropynyl butylcarbamate | 0.1 |
| 21 | Polyacrylamide, C13-14 isoparaffin and Laureth-7 | 0.1 |

### Stability and skin penetration studies of skin care formulations

The formulation after one month of storage was analyzed by high-performance liquid chromatography (HPLC, Shimadzu, Japan) to determine the extent of degradation of ASA to salicylic acid (SA) utilizing a model LC-20AD pump at 1.5 mL $min^{-1}$, a model SPD-20A UV detector at 230 nm and an analytical column (Phenomenex Kinetex C18, 4.6 × 250 mm, pore size 5 μm) combined with a guard column (C18, 4.6 mm i.d, Phenomenex) at 30 °C. The mobile phase comprised 75% phosphate buffer and 25% acetonitrile.

The permeation study was performed with Franz-type diffusion cells (Inline system with 9 mm inline cells, PermeGear). PBS was used as a receptor medium. The receptor medium was circulating by a peristaltic pump (flow 25 μL $min^{-1}$), and the temperature was maintained at 36 °C by circulating water at a constant temperature in the outer jacket of the receiver compartment. The temperature had to be set at 36 °C to produce the temperature reading of the formulation in the receptor compartment at 32 °C. Small epidermis pieces (0.64 $cm^2$) were installed between the donor and receptor compartments of the diffusion cell, with the stratum corneum facing the donor compartment. After 1 h to equilibrate the system, 284 μL

 

of each test substance solution (at 0.1%) was applied to the surface of the epidermis sample separating the two chambers of a diffusion cell. The permeation of each test sample was examined in duplicate. At predetermined time points (2 h), 8 samples from the receptor chamber were automatically taken up to 16 h. At the end of experimentation, the skin surface was washed three times with 3 × 500 μL of PBS. The epidermis was placed in a tube for lysing (5 min, 50 hertz) with 1 mL of methanol and 5 mm disposable stainless steel bead (Tissue Lyser LT, Qiagen). Extraction samples were centrifuged for 5 min at 20 000 rpm. Wash samples and epidermis extractions were analyzed by HPLC.

### *In vivo* testing of skin care formulation

Cosmetic after shave formulation subsequent to safety assessment was tested on two human volunteers with ingrown hair problem. The shaving area was wetted with lukewarm water and shaving cream was applied before shaving with a twin blade. After shave cream was applied once the shaving was completed. This procedure was repeated twice a day for 4 consecutive days. The application area was continuously monitored visually and pictures were taken at regular intervals.

All experiments were performed in compliance with the guideline "Cosmetic Research Ethics Review Method Involving people" (South Africa), and approved by the Faculty of Science Ethics Committee at University of Johannesburg. Informed consents were obtained from human participants of this study.

## 3 Results and discussion

### Nanohybrid formation, morphological and physical properties

The XRD patterns of neat ZnAl-LDH and the LDH–ASA nanohybrid are shown in Fig. 2. The pristine ZnAl-LDH showed a hexagonal lattice with rhombohedral symmetry[28] with a main peak at $2\theta = 11.46°$ (~0.77 nm), which can be attributed to the (003) reflection hydroxyl or carbonate form of LDHs.[20] The sharp and well defined diffraction peaks of the pattern indicate the formation of a hydrotalcite-like structure with good crystallinity. After the intercalation of ASA, the XRD pattern of the nanohybrid retains the major distinctive features of ZnAl-LDH. The intercalation of ASA in ZnAl-LDH, results in a broadened peak around $2\theta = 4.06°$ ($d_{003}$-spacing equivalent 2.18 nm) and a major peak at 9.99° ($d_{003}$-spacing of 0.89 nm). The broadening and shifting of (003) reflection to a lower $2\theta$ angle indicate decreased stacking of layers and increase in the interlayer distance in LDH which may be related to the intercalation of large ASA anions into LDH galleries.[25,29] According to Hu *et al.*,[30] a weak and broadened (003) reflection is exhibited by a very small nano-platelet composed of 1–5 layers. In addition, considering 0.48 nm layer thickness of the LDH sheets, the gallery spacing calculated for the broad reflection is 1.68 nm which may be due to the vertical arrangement of ASA anions in the interlayer regions.

The molecular size of the ASA anion was calculated by using Avogadro Software. According to this calculation, the ASA

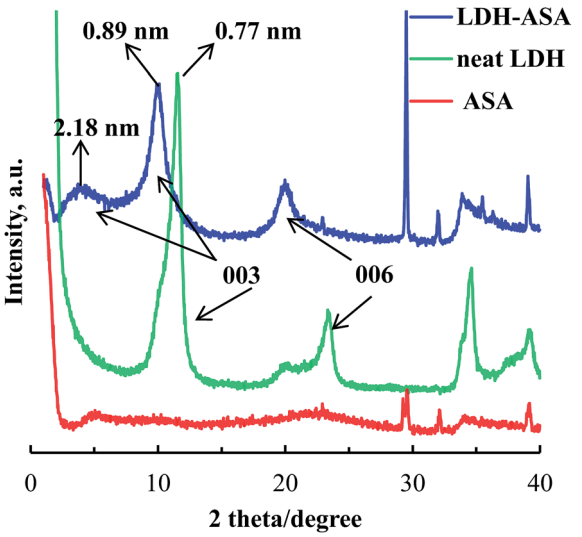


Fig. 2 The XRD patterns of ZnAl-LDH, ASA and LDH–ASA nanohybrid.

molecule is approximately 7.1 Å in length. Based on molecular simulations, Meng *et al.*[25] showed a vertical arrangement of ASA with $COO^-$ group closer to the LDH sheets in intercalated hybrid. However, in our case, the main reflection of LDH–ASA is at 9.99°. This indicates the existence of a predominant phase with interlayer distance of 0.89 nm which could mean that a greater part of ASA is oriented with phenyl ring parallel to the sheets. Kovář *et al.*[31] combined molecular modelling and experimental XRD data for porphyrin intercalated LDH and presented a similar bi-phasic model where some layers are saturated with organic anions and others with original $NO_3^-$ anions. The sharp peak observed at $2\theta = 29°$ suggests the possibility of surface adsorbed ASA species which can affect the release profile of the nanohybrid in the initial hours.

The FTIR spectra of ZnAl-LDH, ASA and the LDH–ASA nanohybrid are shown in Fig. 3. For ZnAl LDH, the broad absorption band between 3400–3500 $cm^{-1}$ is due to the stretching frequency mode of the O–H groups in the brucite-like layer. The shoulder band at 1628 $cm^{-1}$ can be attributed to the bending vibration of water molecules in the interlayer region.[32] Although the starting materials are chloride based, there is a peak at 1359 $cm^{-1}$ normally ascribed to carbonate asymmetric

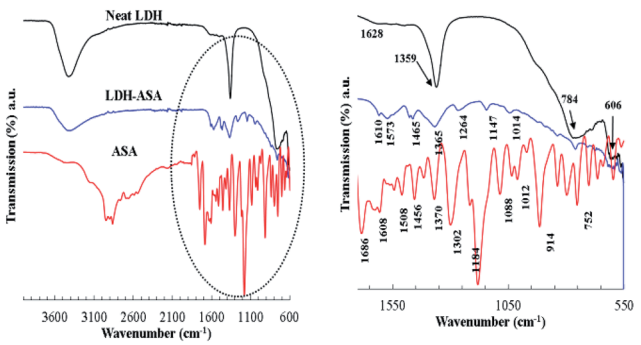


Fig. 3 FTIR spectra of ZnAl-LDH, ASA and LDH–ASA nanohybrid.

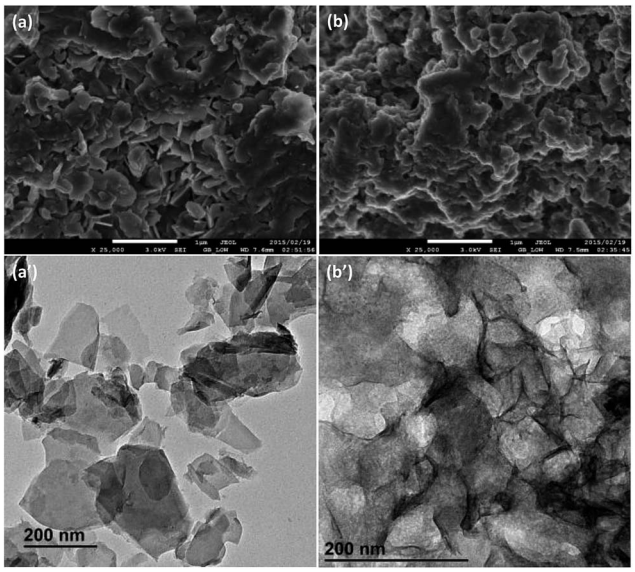


Fig. 4 The SEM and TEM micrographs of unmodified LDH [(a) & (a′)] and LDH–ASA nanohybrid [(b) & (b′)].

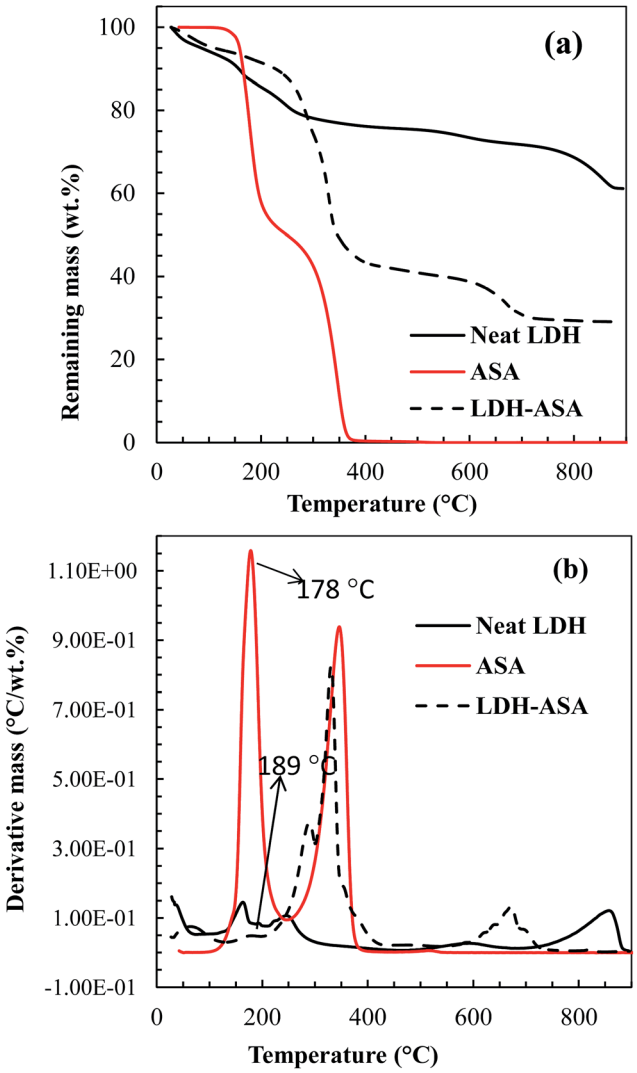


Fig. 5 (a) TG and (b) DTG curves of ZnAl-LDH, ASA and LDH–ASA nanohybrid.

stretching mode which could be explained by the formation of this species during sample preparation.[33] The weak bands around 760 and 600 $cm^{-1}$ can be correlated to the Al–OH and Zn–Al–OH translational and bending vibrations respectively.[34,35] The FTIR spectrum of ASA shows peaks at 1686 and 1456 $cm^{-1}$, which are assigned to the stretching vibration of the C=O bond in the carboxylic group. The peaks at 1508, 1302 and 1184 $cm^{-1}$ correspond to the stretching vibrations of the C=C bonds in an aromatic ring whereas the peaks between 2850 and 2960 $cm^{-1}$ indicate symmetric and asymmetric stretching modes of $-CH_3$ groups.[25] In the case of LDH–ASA nanohybrid, a peak with diminished intensity is observed at a lower wavenumber of 1365 $cm^{-1}$ which may be due to the symmetric stretching vibration of $COO^-$ of intercalated ASA. The peak may also indicate traces of $CO_3^{2-}$ (due to high sensitivity of IR technique, even traces are detected) impurity remaining in the sample which is a common problem with most LDH preparation method including co-precipitation.[36,37] Furthermore, the asymmetric and symmetric stretching modes of the $COO^-$ group observed at 1573 and 1365 $cm^{-1}$ are at lower wave-numbers for the nanohybrid in comparison to the free –COOH functional group in ASA (1686 and 1370 $cm^{-1}$), indicating that the intercalation of ASA in the interlayer space involves a strong hydrogen bond between the layers $COO^-$ groups and hydroxyl groups.[25] Zou *et al.*[38] reported similar shifting of FTIR peaks of carboxylate anions in ZnAl LDHs intercalated with 5-amino salicylate anions. The characteristic M–OH layer lattice vibrations at 764 and 608 $cm^{-1}$ are well defined even in the intercalated sample, indicating the structural stability of LDH during intercalation.[38]

Table 2 Compositional data and apparent formula for the neat LDH and LDH–ASA nanohybrid

| | Zinc to aluminium mol ratio | $x$ | Apparent formula |
|---|---|---|---|
| LDH–ASA | 1.68 | 0.37 | $[Zn_{0.63}Al_{0.37}(OH)_2](ASA)_{0.37}\cdot 0.5H_2O$ |

The structure and morphology of the prepared samples were studied using SEM and TEM. The SEM and TEM images of unmodified LDH [(a) & (a′)] and LDH–ASA nanohybrid [(b) & (b′)], respectively, are presented in Fig. 4.

It can be observed that the neat LDH is composed of lamellar subhedral sheets that are 200–500 nm in size [refer to TEM image (a′)]. The shapes of the ZnAl-LDH particles, however, are not well defined. Distinct platelet edges are not clearly visible in the LDH–ASA nanohybrid sample, as observed in Fig. 4(b′), which could also be correlated with the loss of stacking or increase in disorder as seen from the XRD patterns. Furthermore, the surface of the particles appears to be clean and smooth in the unmodified LDH in comparison to the LDH–ASA nanohybrid. The deposition of a polymer-like coating on the surface is visible for LDH–ASA nanohybrid, which may be due to

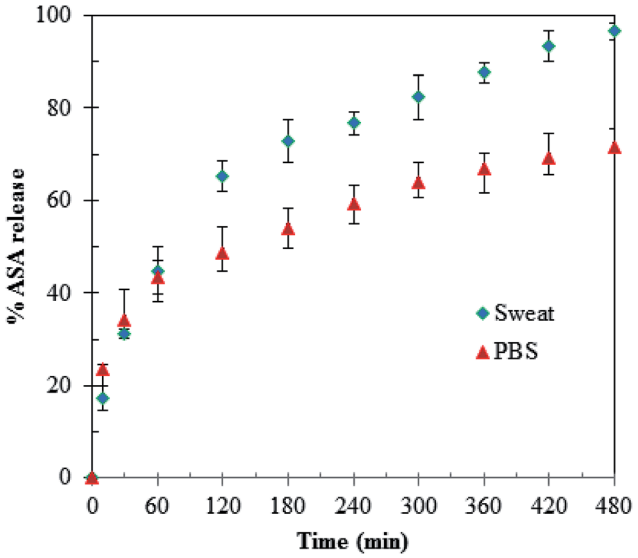


Fig. 6 (a) Release profiles of LDH–ASA nanohybrid in sweat and PBS media measured at 37 °C.

the possible adsorption of the ASA on the outer surface. The increased tendency of particle aggregation in the intercalated sample is also apparent from the TEM image [Fig. 4(b′)].

The chemical composition of LDH–ASA nanohybrid was analyzed by ICP-MS and the results are presented in Table 2. The ICP data are reported as mole ratio relative to aluminium. The LDH precursor used in the study represented by the formula $[M_{1-x}^{2+}M_x^{3+}(OH)_2](CO_3)_{x/2}\cdot nH_2O$, where $x$ quantifies the fractional replacement of Zn by Al ions in the hydroxide sheets. The $x$-value is reported to fall within $0.1 \leq x \leq 0.5$, with pure phases existing for $0.2 \leq x \leq 0.3$.[39] LDH–ASA nanohybrid $x$-value is within what is expected of LDHs. When the $x$-values are lower than 0.33, the Al octahedral is not neighbouring, leading to a high density of Zn octahedral in the brucite-like sheet. In the case of higher values of $x$, the increased number of neighbouring Al octahedral leads to the formation of $Al(OH)_3$.

The TG and corresponding derivative curves of ZnAl-LDH, ASA and LDH–ASA are shown in Fig. 5. ASA exhibits two weight loss events between 120 and 400 °C attributed to the elimination of acetic acid and evaporation of ASA and SA respectively.[25,40] Unmodified LDH shows four weight loss stages. The first stage corresponding to the removal of the surface and interlayer water molecules occurs from 50 °C up to 150 °C.[41] The second event around 245 °C is due to a dehydroxylation process. The third and fourth steps occurring at about 588 and 867 °C involves the oxidative degradation of the anions attached to Zn and Al within the interlayer, respectively.[42] LDH–ASA nanohybrid clearly shows additional weight loss occurring between 200 and 400 °C, which may be attributed to the decomposition of the intercalated ASA. It is also apparent that the decomposition peak temperature of pure ASA increases from 178 °C to 189 °C [refer Fig. 5(b)] after intercalation into the LDH interlayer, indicating the increased thermal stability of ASA in the nanohybrid which could mean that the ASA anions formed a stable conformation in the interlayer spaces of LDH. The

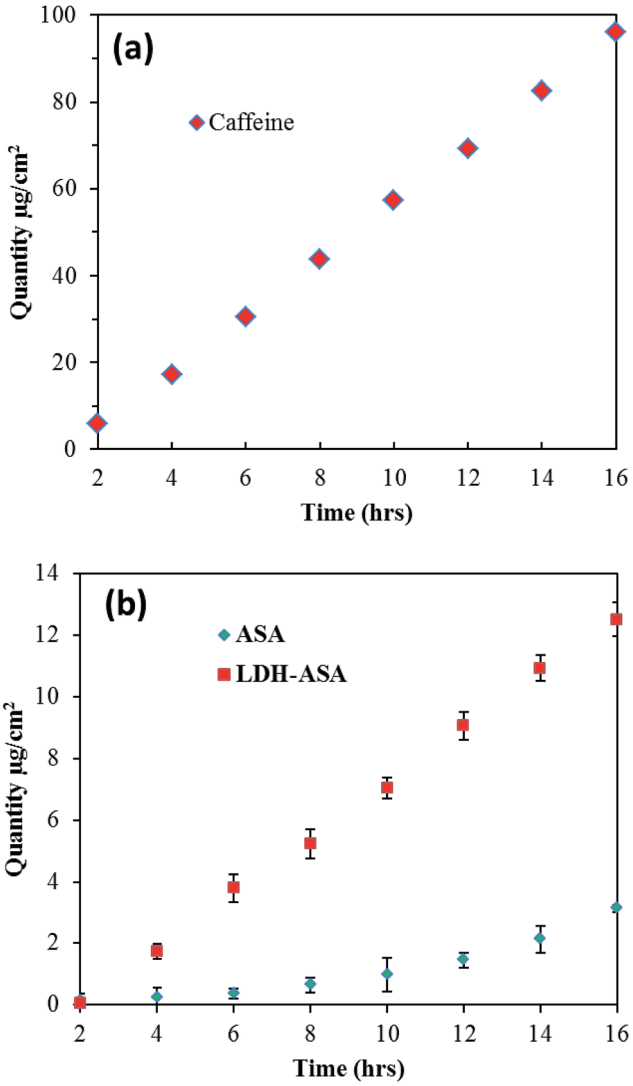


Fig. 7 Cumulative amount penetrated *versus* time for (a) caffeine (standard), (b) pure ASA and the studied LDH–ASA nanohybrid.

residual weight percentage analysis of LDH and the nanohybrid suggest that the total organic component in the hybrid is approximately 32%, although Meng *et al.*[25] observed 26.4% and 28.9% loading of aspirin in LDH hybrids prepared respectively by co-precipitation and reconstruction methods.

### *In vitro* control release study

Preliminary *in vitro* control release studies were performed to observe the release profile of ASA from the LDH–ASA nanohybrid. Drug release patterns from LDH–ASA for 8 h in artificial sweat and PBS media at 37 °C are shown in Fig. 6. From the figure, a rupture or burst release trend is observed for about 46.4% of ASA in the first 60 min, which may be accounted for the loosely bound surface adsorbed ASA. ASA release profile from LDH–ASA nanohybrid shows approximately similar trend in both release media. LDH–ASA nanohybrid in artificial sweat as well as in PBS shows a gradual two step release (refer Fig. 6), with an early fast release, 67.53% for sweat and 51.09% for PBS

Table 3 Permeability coefficient of caffeine, ASA and LDH–ASA and the penetration rate at different time intervals

| Sample | Permeability coefficient ($P_{app}$, cm $h^{-1}$) | Penetration rate (time/h) | | | | | | | |
|---|---|---|---|---|---|---|---|---|---|
| | | 2 | 4 | 6 | 8 | 10 | 12 | 14 | 16 |
| Caffeine | $1.47 \times 10^{-6} \pm 4.94 \times 10^{-7}$ | 5.88 | 17.26 | 30.54 | 43.88 | 57.23 | 69.3 | 82.51 | 96.1 |
| ASA | $3.62 \times 10^{-8} \pm 2.53 \times 10^{-8}$ | 0.24 ± 0.15 | 0.32 ± 0.14 | 0.46 ± 0.13 | 0.64 ± 0.14 | 0.98 ± 0.13 | 1.46 ± 0.15 | 2.13 ± 0.12 | 3.14 ± 0.13 |
| LDH–ASA | $2.48 \times 10^{-7} \pm 2.28 \times 10^{-9}$ | 0.05 ± 0.1 | 1.74 ± 0.6 | 3.80 ± 0.8 | 5.23 ± 0.6 | 7.05 ± 0.5 | 9.07 ± 0.6 | 10.94 ± 0.6 | 12.52 ± 0.3 |

medium in the first 120 min, followed by a relatively slow release, 97.5% for sweat and 74.01% for PBS in the 480 min. The results show a much slower release pattern from ZnAl host layers in comparison to the report by Meng *et al.*,[25] who observed 96.87% release in PBS solution at 300 min. The two step and prolonged release behavior could play key role in the therapeutic cures, as the initial fast release provides the required dosage and the subsequent sustained release continues this dose over extended period of time.[42] The released concentration of ASA from the nanohybrid is significantly slower in PBS solution than in artificial sweat, indicating faster diffusion of ASA from the nanohybrid under skin conditions. The faster release rate in sweat medium could also be attributed to its lower pH (pH = 5.4), which dissolves LDHs slightly thus increasing the diffusion rate of ASA in comparison to PBS medium with neutral pH.[43,44] The release process proceeds along the time period studied, indicating the prolonged and sustained release of ASA from the nanohybrid. When ASA is added directly to a physical mixture, the release is a dissolution process, whereas the release of ASA from LDH–ASA could occur through a diffusion process or an ion-exchange process between the interlayer and the anions from the medium,[45] which makes it a more steady process. The release of ASA under the experimental conditions also indicates that the active molecules formed a stable conformation in the LDH interlayers, making the de-intercalation a slow process.

## Stability and skin penetration studies

In order to confirm the stability of ASA, formulations with initial ASA concentration of 2 wt% were analyzed by HPLC and content of SA, which is one of the decomposition products, was measured after 1 month of storage. Formulation where pure ASA was added showed the presence of 1.2% of SA indicating a faster degradation of ASA whereas the formulation containing LDH–ASA showed only 0.5% of SA suggesting that majority of ASA still exist in its intercalated form. This observation also confirmed the increased structural stability of ASA once intercalated to the LDH interlayers.

Fig. 7 shows the cumulative amount penetrated *versus* time plots for a standard [caffeine as reference, Fig. 7(a)], formulation containing pure ASA and LDH–ASA nanohybrid [Fig. 7(b)]. An automated algorithm was used to calculate the maximum flux ($J_{max}$, μg $cm^{-2}$ $h^{-1}$) and the apparent permeability coefficient ($P_{app}$, cm $h^{-1}$) is shown in Table 3.

As shown in figures and Table 3, the penetration rate of ASA from a formulation containing nanohybrid was approximately 10-fold higher than that of a formulation containing the corresponding weight percentage of pure ASA indicating that the presence of LDH increases the transdermal transport of active molecules.

Furthermore, the linear relationship between the concentrations of ASA permeated and time indicates the steady and efficient release of ASA from the nanohybrid in the formulation [Fig. 7(b)]. Emulsions containing inorganic nanoparticles have previously been reported to increase the penetration of caffeine compared to traditional formulations due to better adhesion of the droplets to the surface.[46] However, due to its rigid structure, the nanoparticles may not penetrate through the corneocytes. Therefore, by acting as reservoir that is strongly anchored to the external skin surface, nanoparticles can then slowly release the active molecules to the skin layers.[43]

It could be that a similar mechanism occurs in our case with the transport of ASA from LDH–ASA nanohybrid. After the initial fast adhesion of LDH–ASA to the skin from the emulsion, the chemical species present in skin wastes, serums and sweats trigger the release of ASA from the nanohybrid through the ion exchange process. In this way, ASA could be slowly diffused out from the ZnAl-LDHs interlayer and delivered into the epidermis. Yang *et al.*[15] proposed similar mechanism for the efficient transdermal penetration of L-ascorbic acid from a ternary nanohybrid of the active, LDH core and $SiO_2$ shell structure. Fig. 8 presents a proposed mechanism (inspired from Yang *et al.*[15]) for the release of ASA from LDH–ASA nanohybrid.

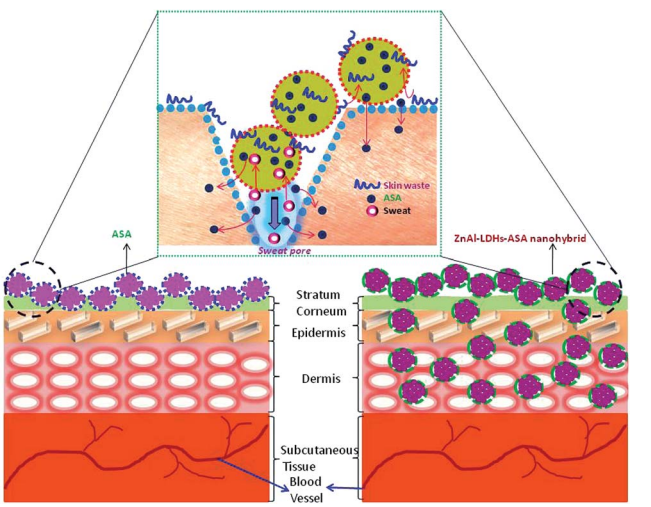


Fig. 8 The proposed skin penetration and release mechanism of ASA from ZnAl-LDH (adapted from Yang *et al.*[15]).


Fig. 9 Representative digital photographs of application area in volunteers 1 (top) and volunteer 2 (bottom) 4 days application of after shave formulations containing pure ASA and LDH–ASA nanohybrid.

In the formulation where pure ASA is used, the bioavailability of ASA will be lower due to the high probability of degradation and chemical instability. The hydrophobicity of pure ASA, which results in less skin absorption, could also be a reason for the lower penetration rate obtained for a formulation with ASA alone.

### *In vivo* studies of skin care formulation

The patch test for a cosmetic product was used to check the compatibility of a formulation with the human skin before its application. The oil/water emulsion topical composition with pure ASA and LDH–ASA nanohybrid was applied for at least twice per day for 4 days and no skin irritation was observed after the application on the razor bumps associated to chin area of 2 human volunteers. Therefore, the developed formulation with the nanohybrid was considered well suited and reasonably safe for consumer use. Commercially available razor bump creams and gels,[47–51] are reported to use active ingredients, such as alcohol and/or ASA, both primarily to reduce an inflammation and infection. Fig. 9 shows digital photographs of affected facial area before and after application of after shave bump creams of neat ASA and LDH–ASA formulation for 4 consecutive days obtained for 2 volunteers.

From the images, it is evident that continuous use of the LDH–ASA nanohybrid formulation reduced the razor bumps and skin became clear after 4 days, when compared to the pure ASA formulation which mimicked commercial after shave cream with ASA concentration in the maximum allowed limit (2%). Therefore, this observation proves that the developed LDH–ASA nanohybrid based formulation is highly efficient in alleviating skin problems in a very short time, when compared to commercial products. This may be due to the high absorption and skin penetration ability of LDH–ASA which is in line with the characterization results.

## 4 Conclusions

Novel nanohybrid materials were developed as high performance cosmeceutical ingredient by the *in situ* intercalation of anti-inflammatory active ASA into ZnAl-LDH. The intercalated ASA showed superior storage and structural stability in formulation when compared to pure ASA. The nanohybrid showed gradual two-step *in vitro* release of ASA up to 8 h under skin conditions indicating excellent controlled release properties. A linear relationship between the cumulative amount of ASA delivered and time obtained from transdermal penetration studies also proved a steady and efficient release of ASA from the nanohybrid in the skin care formulation. A 10-fold increase in percutaneous penetration of ASA from the nanohybrid based formulation was observed and preliminary efficacy results from *in vivo* trials showed its high prospects in curing skin disorders like razor bumps in a short span of time.

## Acknowledgements

Author DM sincerely acknowledge the Directors of Amka Products Pty Ltd, South Africa, for their financial and laboratory facilities. DM also wishes to specially thank Mr Nazir Kalla, Mr Hussain Kalla, Prof. Victor Witlock, Dr Manfred Scriba, Dr James Wesley Smith and the THOR personal care team (France and South Africa). LM, SP, and SSR are further thankful to the Department of Science and Technology and the Council for Scientific and Industrial Research for laboratory and characterization facilities and financial support.

## References

1 Q. Wang and D. O'Hare, *Chem. Rev.*, 2012, **112**, 4124–4155.
2 A. N. Ay, D. Konuk and B. Zumreoglu-Karan, *Mater. Sci. Eng., C*, 2011, **31**, 851–857.
3 J. Chakraborty, S. Roychowdhury, S. Sengupta and S. Ghosh, *Mater. Sci. Eng., C*, 2013, **33**, 2168–2174.
4 U. Costantino and M. Nochetti, in *Layered double hydroxides: present and future*, ed. V. Rives, Nova Science Publishers, New York, 2001, ch. 12, pp. 435–468.
5 A. I. Khan, L. Lei, A. J. Norquist and D. O'Hare, *Chem. Commun.*, 2001, **22**, 2342–2343.

6 U. Costantino, V. Ambrogi, M. Nocchetti and L. Perioli, *Microporous Mesoporous Mater.*, 2008, **107**, 149–160.
7 V. Ambrogi, G. Fardella, G. Grandolini, M. Nocchetti and L. Perioli, *J. Pharm. Sci.*, 2003, **92**, 1407–1418.
8 V. Ambrogi, G. Fardella, G. Grandolini, L. Perioli and M. C. Tiralti, *AAPS PharmSciTech*, 2002, **3**, 26.
9 V. Ambrogi, G. Fardella, G. Grandolini and L. Perioli, *Int. J. Pharm.*, 2001, **220**, 23–32.
10 J.-H. Choy, J.-S. Jung, J.-M. Oh, M. Park, J. Jeong, Y.-K. Kang and O.-J. Han, *Biomaterials*, 2004, **25**, 3059–3064.
11 J.-H. Choy and Y.-H. Son, *Bull. Korean Chem. Soc.*, 2004, **25**, 122–126.
12 M. Wei, M. Pu, J. Guo, J. B. Han, F. Li, J. He, D. G. Evans and X. Duan, *Chem. Mater.*, 2008, **20**, 5169–5180.
13 C. Del Hoyo, *Appl. Clay Sci.*, 2007, **36**, 103–121.
14 U. Costantino, F. Leroux, M. Nochetti and C. Mpusty, in *Clay Science – Handbook of Clay Science: Techniques and Applications*, ed. F. Bergaya and G. Lagaly, Elsevier, Amsterdam, 2013, ch. 6, pp. 765−791.
15 J. H. Yang, S. Y. Lee, Y. S. Han, K. C. Park and J. H. Choy, *Bull. Korean Chem. Soc.*, 2003, **24**, 499–503.
16 J. H. Choy, Y. S. Han, S. H. Hwang and C. W. Lee, *US Pat.*, WO2003011233 A1, 2003.
17 L. Perioli, V. Ambrogi, B. Bertini, M. Ricci, M. Nocchetti, L. Latterini and C. Rossi, *Eur. J. Pharm. Biopharm.*, 2006, **62**, 185–193.
18 L. Perioli, V. Ambrogi, C. Rossi, B. Bertini, L. Latterini, M. Nocchetti and U. Constantino, *J. Phys. Chem. Solids*, 2006, **67**, 1079–1083.
19 V. Ambrogi, L. Perioli, C. Rossi and L. Latterini, *J. Phys. Chem. Solids*, 2012, **73**, 94–98.
20 L. Perioli, V. Ambrogi, M. Nocchetti, C. Pagano, E. Massetti and C. Rossi, *J. Pharm. Sci.*, 2015, **11**, 3904–3912.
21 R. Amann and B. A. Peskar, *Eur. J. Pharmacol.*, 2002, **447**, 1–9.
22 L.-e. Dong, G. Gou and L. Jiao, *Acta Pharm. Sin. B*, 2013, **3**, 400–407.
23 L.-L. Li, X.-C. Zhan and J.-L. Tao, *Arch. Pharmacal Res.*, 2008, **31**, 381–389.
24 L. Dong, G. Gou and L. Jiao, *Acta Pharm. Sin. B*, 2013, **3**, 400–407.
25 Z. Meng, X. Li, F. Lv, Q. Zhang, P. K. Chu and Y. Zhang, *Colloids Surf., B*, 2015, **135**, 339–345.
26 D. Mosangi, S. Kesavan Pillai, L. Moyo and S. S. Ray, *RSC Adv.*, 2016, **6**, 77709–77716.
27 M. R. C. Marques, R. Loebenberg and M. Almukainzi, *Dissolution Technol.*, 2011, **18**, 15–28.
28 A. Vaccari, *Catal. Today*, 1998, **41**, 53–71.
29 G. Fan, F. Li, D. G. Evans and X. Duan, *Chem. Soc. Rev.*, 2014, **43**, 7040–7066.
30 G. Hu, N. Wang, D. O'Hare and J. Davis, *J. Mater. Chem.*, 2007, **17**, 2257–2266.
31 P. Kovář, M. Pospíšil, E. Káfuňková, K. Lang and F. Kovanda, *J. Mol. Model.*, 2010, **16**, 223–233.
32 Y. Wang, P. Wu, Y. Hou, N. Zhu and Z. Dang, *Ind. Eng. Chem. Res.*, 2012, **51**, 11128–11136.
33 M. A. Araméndıa, V. Borau, C. Jiménez, J. M. Marinas, J. R. Ruiz and F. J. Urbano, *J. Solid State Chem.*, 2002, **168**, 156–161.
34 T. J. Kloprogge, R. L. Frost and L. Hickey, *J. Raman Spectrosc.*, 2004, **3**, 967–974.
35 M. Z. B. Hussein, Z. Zainal, A. H. Yahaya and A. B. A. Aziz, *Mater. Sci. Eng., B*, 2002, **88**, 98–102.
36 W. T. Reichle, *J. Catal.*, 1985, **94**, 547–557.
37 S. P. Newman and W. Jones, *New J. Chem.*, 1998, **22**, 105–115.
38 K. Zou, H. Zhang and X. Duan, *Chem. Eng. Sci.*, 2007, **62**, 2022–2031.
39 F. Cavani, F. Trifirò and A. Vaccari, *Catal. Today*, 1991, **11**, 173–301.
40 Y. A. Ribeiro, A. C. F. Caires, N. Boralle and M. Ionashiro, *Thermochim. Acta*, 1996, **279**, 177–181.
41 S. Carlino and M. J. Hudson, *J. Mater. Chem.*, 1994, **4**, 99–104.
42 N. Voyer, A. Soisnard, S. J. Palmer, W. N. Martens and R. L. Frost, *J. Therm. Anal. Calorim.*, 2009, **96**, 481–485.
43 X. Kong, L. Jin, M. Wei and X. Duan, *Appl. Clay Sci.*, 2010, **49**, 324–329.
44 F. Barahuie, M. Z. Hussein, S. Fakurazi and Z. Zainal, *Int. J. Mol. Sci.*, 2014, **15**, 7750–7786.
45 X. Wu, H. Li, S. Song, R. Zhang and W. Hou, *Int. J. Pharm.*, 2013, **454**, 453–461.
46 J. Frelichowska, M.-A. Bolzinger and J.-P. Valour, *Int. J. Pharm.*, 2009, **368**, 7–15.
47 G. Mildenberger and B. Mildenberger, *US Pat.*, 6503496, 2003.
48 W. E. Bliss, *US Pat.*, 4228163, 1980.
49 N. Perricone, *Cutis*, 1993, **52**, 232–235.
50 S. A. Victor, *US Pat.*, 5204093, 1993.
51 P. K. Perry, F. E. Cook-Bolden, Z. Rahman, E. Jones and S. C. Taylor, *J. Am. Acad. Dermatol.*, 2002, **46**, S113–S119.